Chemical ordering dependence of interlayer exchange coupling in Co-Mn-Si/Cr/Co-Mn-Si trilayer structures

S. Bosu, Y. Sakuraba, K. Saito, H. Wang, S. Mitani, and K. Takanashi
Institute for Materials Research, Tohoku University, 2-1-1 Katahira, Aoba-Ku, Sendai 980-8577, Japan
(Received 7 September 2009; revised manuscript received 5 December 2009; published 17 February 2010)

The effect of chemical ordering of a half-metallic full-Heusler alloy Co_2MnSi (CMS) on interlayer exchange coupling (IEC) behavior was investigated in Co-Mn-Si(20 nm)/Cr(1.2 nm)/Co-Mn-Si(7 nm) trilayers. Two types of experimental investigations were employed, namely, the variations in IEC with changing the annealing temperature of the bottom CMS from room temperature to 500 °C and with changing the Co concentration in top and bottom Co-Mn-Si layers. The 90° coupling parameter J_2 and the bilinear coupling parameter J_1 were estimated from the numerical simulations of magnetization curves. Only the strong 90° coupling with almost the same strength was observed in both the completely $B2$ ordered and in a mixture of ordered $L2_1$ and $B2$ structures. The degree of $B2$ ordering as well as the strength of 90° coupling was observed to decrease simultaneously with the Co concentration in Co-Mn-Si and 180° coupling appeared in highly Co antisite defective ($A2$) structures, i.e., for the Co concentration over 73 at. %. This observation showed a clear relationship between the degree of $B2$ ordering and the IEC behavior in full-Heusler Co-Mn-Si-based structures.

DOI: 10.1103/PhysRevB.81.054426 PACS number(s): 75.50.Cc

I. INTRODUCTION

The discovery of antiferromagnetic interlayer exchange coupling (IEC) in Fe/Cr/Fe nanostructures in 1986 (Ref. 1) and accordingly the manifestation of giant magnetoresistance (GMR) effect[2] triggered great interest in the intensive study of the physics of metallic layered structures. Later the oscillation behavior of IEC as well as magnetoresistance with nonmagnetic spacer thickness was reported in ferromagnetic/nonferromagnetic multilayer structures.[3] Furthermore, a biquadratic contribution to the IEC in Fe-Cr-Fe-layered structures was observed, leading to an equilibrium canting angle near 90° between the magnetization directions in (the) ferromagnetic layers.[4] Until now, there have been a great number of experimental investigations of the bilinear and biquadratic coupling especially in transition-metal ferromagnet and their alloy-based layer structures.[5–11] Nowadays, the short- and long- period oscillations of bilinear coupling are well described by theoretical models based on Rudermann-Kittel-Kasuya-Yosida picture and quantum well approach.[12,13] At the same time, different models accounting for intrinsic and extrinsic contributions of biquadratic coupling have also been proposed,[14,15] however, many questions remain to be clarified.

Given the theoretical predictions of 100% spin polarization in an entire class of materials, half-metallic full-Heusler compounds are a promising class of materials for future spintronic applications.[16] Among them, cobalt-based full-Heusler compounds, in particular, Co_2MnSi (CMS) and Co_2MnGe, have remarkably high Curie temperatures well above RT and high spin polarizations.[17,18] Half-metallic full-Heusler alloy CMS has already been demonstrated as a useful material for applications in spin electronics such as tunneling magnetoresistance (TMR) effect.[19,20] The enhancement of the resistance change area product in CPP GMR was also reported in previous studies in epitaxially grown CMS-based trilayers.[21–23] However, those works focus only on transport properties, the IEC behavior in full-Heusler alloy-based ferromagnetic systems is still poorly understood.[24,25] Recently, we reported strong 90° coupling ($J_2=-1.85$ erg/cm^2) with a long oscillation period (3.3–3.5 nm) in epitaxial CMS/Cr/CMS trilayer structures with no sign of contribution by 180° coupling.[26–28] In our very recent studies, dominating 90° coupling with no sign of 180° coupling has also been reported in fully epitaxial CMS/Cr/Fe and $Co_2MnAl/Cr/Co_2MnAl$ trilayer structures.[29,30] The relative magnetization orientation of two CMS layers of about 90° was also confirmed in CMS(20 nm)/Cr(1.2 nm)/CMS(10 nm) trilayer by polarized neutron reflectivity measurement.[31] This is completely a novel behavior of IEC and the origin of this behavior remains an open question.

The full-Heusler alloys, which have a general formula X_2YZ and crystallized in the $L2_1$ structure, may also grow in the chemically ordered $B2[X_2(Y,Z)]$ or disordered $A2$ [X, Y, Z] structure, where in $B2$ and $A2$ structures Y and Z, and X, Y, and Z are randomly substituted, respectively. For spin transport processes, the chemical ordering and the interdiffusion at the interfaces in thin films combining Heusler alloys with other materials has a great importance. A very recent study indicated that $A2$-type (chemical) disordering of CMS led to an immense reduction in TMR ratio.[32] However, there has been no systematic experimental investigation of the effect of chemical ordering on IEC to date. In all of our reported studies of IEC in trilayer structures the full-Heusler alloys CMS and CMA films were grown in $B2$ structure. Therefore, only 90° coupling has been observed when one of the ferromagnetic layers is Co-based full-Heusler alloy with $B2$ structure.

In the present study, we have investigated the effect of chemical ordering on IEC behavior in CMS/Cr/CMS trilayers in two ways, i.e., by changing the annealing temperatures for the bottom CMS from 100 to 500 °C and by increasing the Co concentrations in the top and bottom CMS layers [i.e., increasing the Co antisite ($A2$-type) defects]. In this study, we have found the clear relationship between the chemical ordering of CMS and the IEC behavior in trilayers.

In Sec. II of this paper, sample preparation and measurement methods are outlined. The basic formalism of numerical simulations method is briefly explained in Sec. III, and results of structural and magnetic properties are shown in Sec. IV. Section V contains discussion and the overall study is summarized in Sec. VI.

II. SAMPLE PREPARATION AND EXPERIMENTAL METHOD

All the samples were grown by an ultrahigh vacuum compatible dc-sputtering method with a base pressure less than 1×10^{-7} Pa. A stacking structure of Cr(5 nm)/Au(30 nm)/Cr(15 nm)/CMS(20 nm)/Cr(1.2 nm)/CMS(7 nm)/Au cap was prepared on a MgO (001) substrate. The Cr has small lattice misfits with both CMS (1.9%) and MgO (3.4%), i.e., in this stacking structure the lattice misfits among all neighboring layers are (made up) always less than 4%. Thus, the epitaxial relationship of MgO(001)⟨100⟩//CMS(001)⟨110⟩//Cr(001)⟨110⟩//CMS(001)⟨110⟩ was achieved in this stacking structure during the preparation of samples. First, a 10×10 mm^2 MgO substrate was annealed at 600 °C to remove surface contamination. To improve the surface morphology Cr and Au buffer layers were deposited at room temperature (RT) and then annealed at 300 °C for 1 h. After that, the bottom CMS layer (20 nm) was deposited on the Cr buffer at room temperature to get the high crystalline structure and flat surface. In the study of annealing temperature dependence, the Cr buffer and the bottom CMS were annealed for 1 h at different annealing temperatures T_{ann}(=100–500 °C). On the other hand, for the Co concentration dependence study, they were only annealed at 300 °C. A Cr spacer and the top CMS layers were deposited at room temperature to avoid interdiffusion between them. Note that, the spacer thickness was set at t_{Cr}=1.2 nm throughout the whole study. This typical thickness of Cr spacer signifies the maximum strength of biquadratic coupling in CMS/Cr/CMS trilayers.[26] Finally, a Au-cap layer of 3 nm was deposited at RT. A $Co_{46}Mn_{27}Si_{27}$ alloy target was used in preparing CMS films to obtain nearly stoichiometric composition. In the study of Co concentration dependence, top and bottom $Co_{2+x}MnSi$ layers were prepared by the codeposition technique from $Co_{46}Mn_{27}Si_{27}$ and Co targets by adjusting the input sputtering power onto each target. The compositions of CMS films were determined by inductively coupled plasma (ICP) mass spectroscopy and electron probe microanalysis (EPMA). The composition of the film deposited from $Co_{46}Mn_{27}Si_{27}$ was found to be $Co_{53.3}Mn_{22.1}Si_{24.6}$. The magnetic behavior was investigated by a vibrating sample magnetometer at room temperature, by applying the external magnetic field along the CMS ⟨110⟩, the easy magnetization direction of CMS. The structure and the average surface roughness were investigated by x-ray diffraction (XRD) and atomic force microscopy (AFM), respectively.

III. NUMERICAL SIMULATION METHOD

M-H loops are simulated by using a numerical-simulation model based on three major energy expressions, i.e., the magnetic anisotropy energy (E_K), Zeeman energy (E_Z), and the exchange coupling energy (E_J). The total energy is expressed as follows:

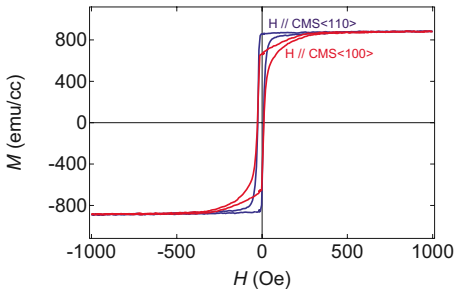

FIG. 1. (Color online) *M-H* loops of single CMS(20 nm) layer for measurement along easy (⟨110⟩) and hard (⟨100⟩) axes.

$$E_T = E_K + E_Z + E_J, \tag{1}$$

where

$$E_K = K_a t_a \sin^2\alpha\cos^2\alpha + K_b t_b \sin^2\beta\cos^2\beta,$$

$$E_Z = -M_a t_a H\cos\alpha - M_b t_b H\cos\beta,$$

$$E_J = -J_1\cos(\alpha-\beta) - J_2\cos^2(\alpha-\beta).$$

Here, K, M, and t are the first-order cubic magnetocrystalline anisotropy constant, the saturation magnetization, and the thickness, respectively, of CMS layers. Subscripts "a" and "b" represent the bottom and top CMS, respectively. H is the applied magnetic field. α (or β) is the angle between the direction of H and M in the bottom (or top) CMS layer. J_1 and J_2 are the bilinear and the biquadratic coupling energies, respectively. Positive J_1 stands for ferromagnetic coupling, while negative J_1 and negative J_2 correspond to 180° and 90° configurations, respectively. For simulating magnetization curves, the minimization of the total energy of Eq. (1) is considered. The values of coupling parameters J_1 and J_2 are evaluated by comparing the simulation results with measured *M-H* loops. The strength of coupling contains uncertainty of about ±5–10 %. In all of our simulations only half of the *M-H* loop is considered for simplicity.

The magnetization values M_a and M_b are estimated from the measurement of *M-H* loops along easy axis for single and trilayer samples. The first-order cubic anisotropy constant K is determined from the measurement of *M-H* loops with applied field along the easy and hard axes for single CMS layer, as shown in Fig. 1. It is to be noted here that no contribution of in-plane uniaxial anisotropy energy was detected in single CMS layer for the measurement of *M-H* loops along two different easy axes.

IV. RESULTS

A. Annealing temperature dependence

1. Structural characterization

The x-ray diffraction profiles for the bottom layer of CMS(20 nm) at different T_{ann} are shown in Fig. 2. The pres-

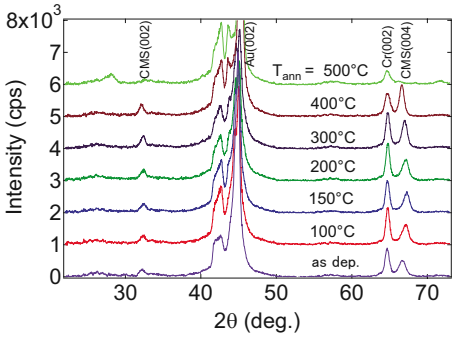

FIG. 2. (Color online) XRD patterns for single CMS layer as deposited to T_{ann}=100–500 °C.

ence of diffraction peaks from only (001) direction for all prepared samples indicates (001)-oriented fully epitaxial growth. The Cr (002) peak intensity at T_{ann}=400 °C is slightly less than those for T_{ann}<400 °C. This might be due to small interdiffusion between the Cr buffer and the bottom CMS layer. A strong interdiffusion seems to occur (between the Cr buffer and the bottom CMS layer) at T_{ann}=500 °C. The absence of CMS peaks and the appearance of a new peak around 2θ=28° at T_{ann}=500 °C indicate that CMS disappears and another phase exists.

T_{ann} dependence of the long-range order parameter (S) for a single CMS(20 nm) and the average surface roughness (R_a) for top and bottom CMS layers film are plotted in Figs. 3(a) and 3(b), respectively. The S for the $B2$ and $L2_1$ structures of CMS were estimated using following formulae:

$$S^2_{L2_1} = \frac{I_{obs}(111)/I_{obs}(220)}{I_{cal}(111)/I_{cal}(220)}, \tag{2}$$

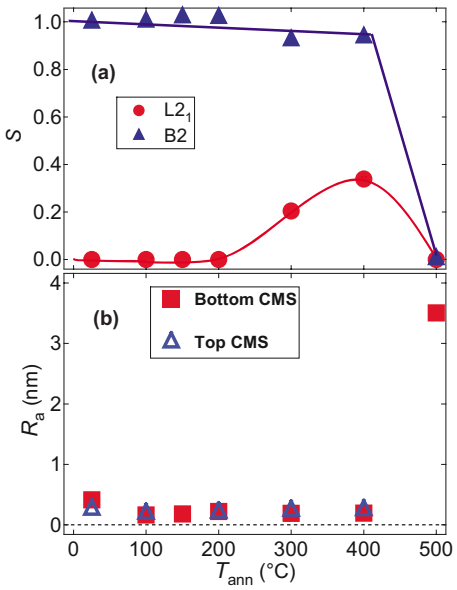

FIG. 3. (Color online) Annealing temperature (T_{ann}) dependence of long-range order parameter (S) (a) for single CMS layer and surface average roughness (R_a) (b) for top and bottom CMS layers.

$$S^2_{B2} = \frac{I_{obs}(200)/I_{obs}(400)}{I_{cal}(200)/I_{cal}(400)}, \tag{3}$$

where, $I(111)$ and $I(200)$ are superlattice peak intensities, whereas $I(220)$ and $I(400)$ are fundamental peak intensities of CMS. The subscripts "*obs*" and "*cal*" represent the experimentally observed and calculated intensities, respectively.

The S of CMS(20 nm) single films evaluated from XRD, plotted in Fig. 3(a), confirmed perfect $B2$ ordering even for the as-deposited sample. The partial $L2_1$ ordering appeared at T_{ann} higher than 200 °C and had a maximum at 400 °C. No ordered structure was obtained at T_{ann}=500 °C. Therefore, for preparation of trilayers, a T_{ann} up to 400 °C was considered. In Fig. 3(b), the magnitude of surface roughness (R_a) for the top and bottom CMS layers shows an almost flat surface ($R_a \sim 0.2$ nm) for T_{ann}=RT to 400 °C.

2. Interlayer exchange coupling behavior

Figure 4 shows the experimental (open circles) and simulated (line) M-H loops of the CMS/Cr/CMS trilayers with bottom CMS T_{ann}=RT to 400 °C. From the magnetization measurement of single and trilayer samples, the saturation magnetizations M_a and M_b are estimated to be M_a=M_b =840 emu/cc for RT deposition and M_a=M_b=880 emu/cc for others ($T_{ann} \sim$ 100–400 °C). The cubic magnetocrystalline anisotropy constants K_a=K_b=-3×10^4 erg/cm^2 are used for all the samples. All the experimental M-H loops with applied field along easy axis of CMS show a remanence M_r/M_s ratio of 0.74, which is the representative point of 90° coupling: the bottom CMS layer has magnetization of about 74% in total magnetization and thus the M_r/M_s becomes ~0.74 when the magnetizations for the top and bottom FM layers are perpendicularly aligned. Therefore, in simulating M-H loops, it is reasonable to consider J_1=0 for all the samples. In Fig. 4(a) the magnetic behavior for RT deposited sample is simulated with J_2=−0.76 erg/cm^2, whereas for others [Figs. 4(b)–4(e)] with J_2=−1 erg/cm^2, which might be due to the slightly large surface roughness of the bottom CMS layer in the as-deposited state, as shown in Fig. 3. The M-H loops for these trilayer samples are also measured and simulated along two different easy axes as well as along the hard axis of CMS. Figures 5(a) and 5(b) show the measured and simulated M-H loop with H applied along two different easy directions of CMS in CMS/Cr/CMS trilayer for as-deposited case. Two identical M-H loops represent negligible contribution of in-plane uniaxial anisotropy energy in such structures. Figure 5(c) represents the M-H loop along the hard-axis measurement and it is also simulated by substituting the Zeeman energy term in Eq. (1) by E_Z=$-M_a t_a H\cos(\alpha-\pi/4)-M_b t_b H\cos(\beta-\pi/4)$ and considering same set of parameters as used in the simulation along easy axis. The corresponding value of M_r/M_s in the M-H loop along hard axis is about 0.707 for 90° coupling. However, no significant change in the magnetization curve indicates the strength of 90° coupling ($|J_2|$=0.76 erg/cm^2) is much higher than the anisotropy energy ($|Kt|$ =0.081 erg/cm^2) contribution.

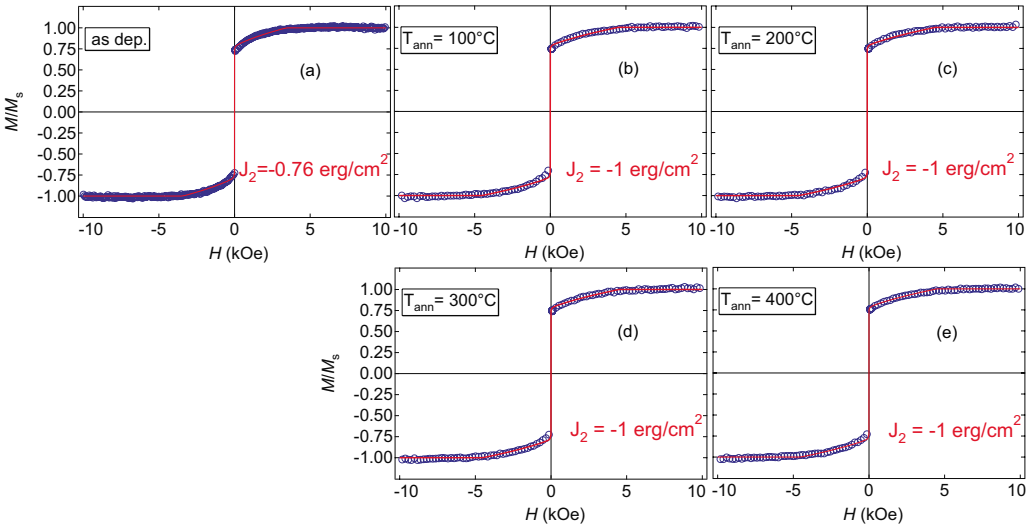

FIG. 4. (Color online) *M-H* loops of CMS(20 nm)/Cr(1.2 nm)/CMS(7 nm) trilayers for bottom CMS(20 nm) (a) as deposited, (b) T_{ann}= 100 °C, (c) T_{ann}=200 °C, (d) T_{ann}=300 °C, and (e) T_{ann}=400 °C, respectively. The open circles and the lines represent the experimental and numerical-simulation results, respectively.

Therefore, the numerical simulations confirm that only 90° coupling dominates in all cases, and there is no significant change in the strength and type of the coupling with T_{ann}. This demonstrates that the IEC behavior does not depend on whether the structure is *B*2 or a mixture of the $L2_1$ and *B*2 ordered structures in this study.

B. Co concentration dependence

1. Structural characterization

Table I shows the film compositions of Co-Mn-Si at. % analyzed by ICP and EPMA techniques. The Co concentration (*X*) in the Co-Mn-Si structure successively increases from 53.3 to 80.4 at. %. The XRD patterns for Co-Mn-Si/Cr/Co-Mn-Si trilayers with *X* from 53.3 to 80.4 at. % are shown in Fig. 6. The presence of diffraction peaks from only (001) direction confirms (001)-oriented fully epitaxial growth without any phase separation. Figure 7 shows the lattice constant of CMS estimated from (004) peak as a function of the *X*. A clear linear dependence of lattice constant with *X* following Vegard's law was confirmed, suggesting the occupation of excess Co atoms to Mn and Si sites. The sample with $X \sim 80.4$ at. % shows the opposite behavior, i.e., the (004) peak position shifts to a lower angle indicating that the single bcc face of *B*2 structure is not stable and creates small phase separation. With increasing *X*, the (002) superlattice peak gradually decreases and vanishes around 78.2 at. %. All these observations indicate that additional Co atoms well occupy the Mn and/or Si sites and form Co antisite defects as expected. The full width at half maximum (FWHM) of the rocking curve (left part) for the CMS (004) peak and the average surface roughness R_a (right part) for the top layer are plotted against *X* in Fig. 8. Both the values of FWHM and R_a keep small for *X* up to 78.2 at. %. Therefore, the structural and surface qualities of the film show no remarkable change with *X* and do not affect the *X* dependence of IEC behavior.

2. Interlayer exchange coupling behavior

Typical simulation results (lines) of experimental *M-H* loops (open circles) for six samples of CMS/Cr/CMS trilayers with different *X* values are shown in Figs. 9(a)–9(f). In Figs. 9(a)–9(c), the experimental remanence M_r/M_s ratio is always ~0.74, representing 90° coupling as explained ear-

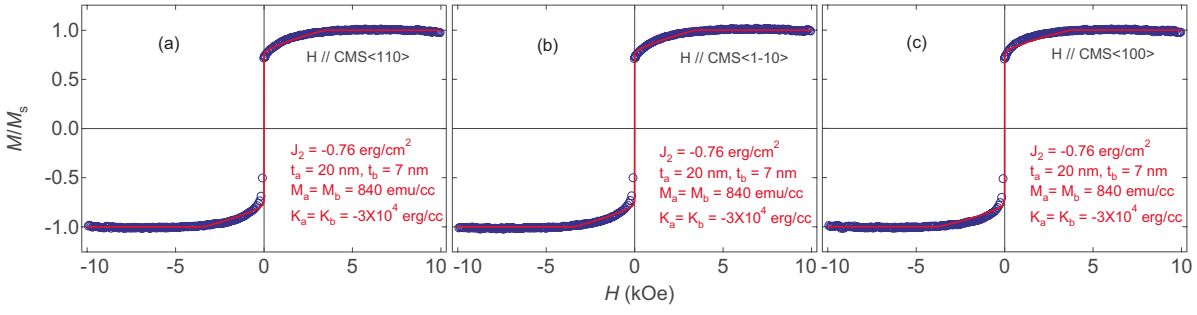

FIG. 5. (Color online) *M-H* loops of CMS(20 nm)/Cr(1.2 nm)/CMS(7 nm) trilayers for as deposited case with *H* applied along CMS (a) ⟨110⟩ easy, (b) ⟨1−10⟩ easy, and (c) ⟨100⟩ hard axes. The open circles and the lines represent the experimental and numerical simulation results, respectively.

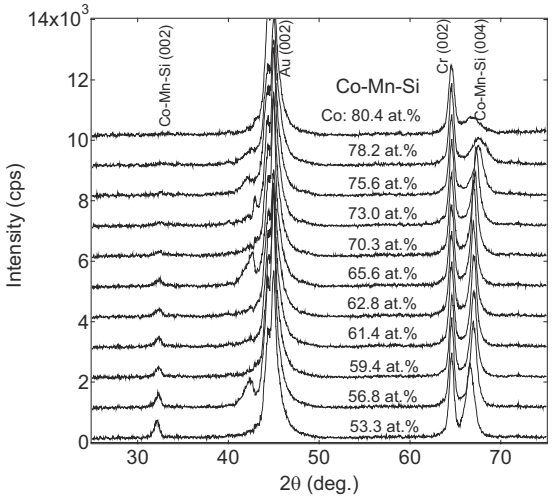

FIG. 6. XRD patterns for Co-Mn-Si/Cr/Co-Mn-Si trilayers with Co concentration of 53.3–80.4 at. %.

lier. In Figs. 9(d)–9(f), however, the M_r/M_s ratio is always smaller than 0.74 and larger than the typical value M_r/M_s ($\sim$0.48) for the 180° coupling, indicating that 90° (coupling) and 180° coupling are comparable. The parameters considered in simulations are $M_a=M_b=950$ emu/cc for $X=53.3-78.2$ at. %, $K_a=K_b=-3\times10^4$ erg/cc for $X=53.3-73$ at. %, and $K_a=K_b=-5.6\times10^4$ erg/cc for $X=75.6$ and 78.2 at. %. These parameters are reasonable because the experimental saturation magnetization M_s is 950 ± 20 emu/cc, and the cubic anisotropy constant K remains in the same order in this range of X. For $X=80.4$ at. %, however, the estimated values of magnetization are $M_a=M_b=880$ emu/cc. The cubic anisotropy constant for this sample was determined to be $K=-6.8\times10^3$ erg/cc. The simulation results show good agreement with the measured M-H loops for all the samples. As shown in Figs. 9(a)–9(c) the M-H loops can be simulated with $J_1=0$ and only changing the strength of 90° coupling, i.e., values of J_2. On the other hand, the consideration of both 90° and 180° coupling (i.e., $-J_2$ and $-J_1$) is required in simulating the M-H loops shown in Figs. 9(d)–9(f).

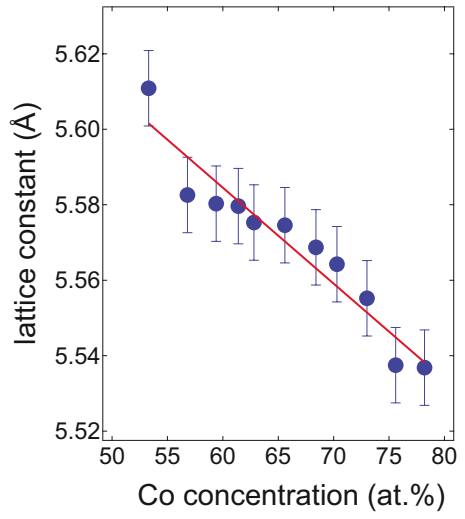

FIG. 7. (Color online) Lattice constant of CMS is plotted against Co concentration in Co-Mn-Si/Cr/Co-Mn-Si trilayers. The line indicates declining characteristics of lattice constant of CMS with Co concentration.

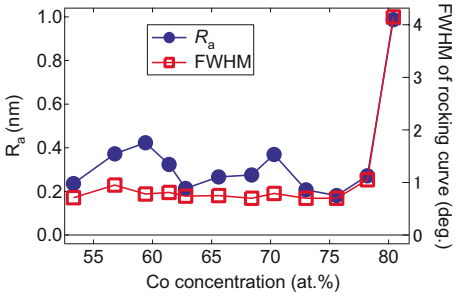

FIG. 8. (Color online) Average surface roughness (R_a) of the top layer and the FWHM of rocking curve of CMS (004) peak are plotted as a function of Co concentration in Co-Mn-Si/Cr/Cr/Co-Mn-Si trilayers.

The intensity ratio of $B2$ superlattice peak to $A2$ fundamental peak, $I(002)/I(004)$, measured by XRD and the values of J_1 and J_2 evaluated from numerical simulations of Co-Mn-Si/Cr/Co-Mn-Si trilayers are plotted as a function of X in Figs. 10(a) and 10(b), respectively. The intensity ratio $I(002)/I(004)$, i.e., the degree of $B2$ ordering, decreases with increasing X and disappears for very high X over 75 at. % [Fig. 10(a)]. Likewise, the 90° coupling strength J_2 decreases in a similar fashion with increasing X and shows a minimum at X of about 70.3 at. % [Fig. 10(b)]. Afterwards, the contribution of negative J_1, i.e., 180° coupling appears for Co-Mn-Si layers with highly Co antisite defective ($A2$) structures. According to the IEC behavior, Fig. 10(b) can be divided into two parts: one is X from 53.3 to 70.3 at. % and the other is from 75.6 to 80.4 at. %. In the first part only 90° coupling dominates and decreases monotonically with X, while in the other, the contribution of 180° coupling arises. The coupling behavior in the latter is common in transition-metal ferromagnet-based thin films, while the former is not familiar in such systems.

TABLE I. Co-Mn-Si film compositions (at.%) analyzed by ICP and EPMA.

Co (at.%)	Mn (at.%)	Si (at.%)
53.3	22.1	24.6
56.8	20.4	22.8
59.4	19.2	21.4
61.4	17.7	20.9
62.8	17.2	20.0
65.6	15.6	18.8
68.4	13.9	17.7
70.3	13.7	16.0
73.0	12.7	14.3
75.6	10.8	13.6
78.2	9.8	12.0
80.4	9.0	10.6

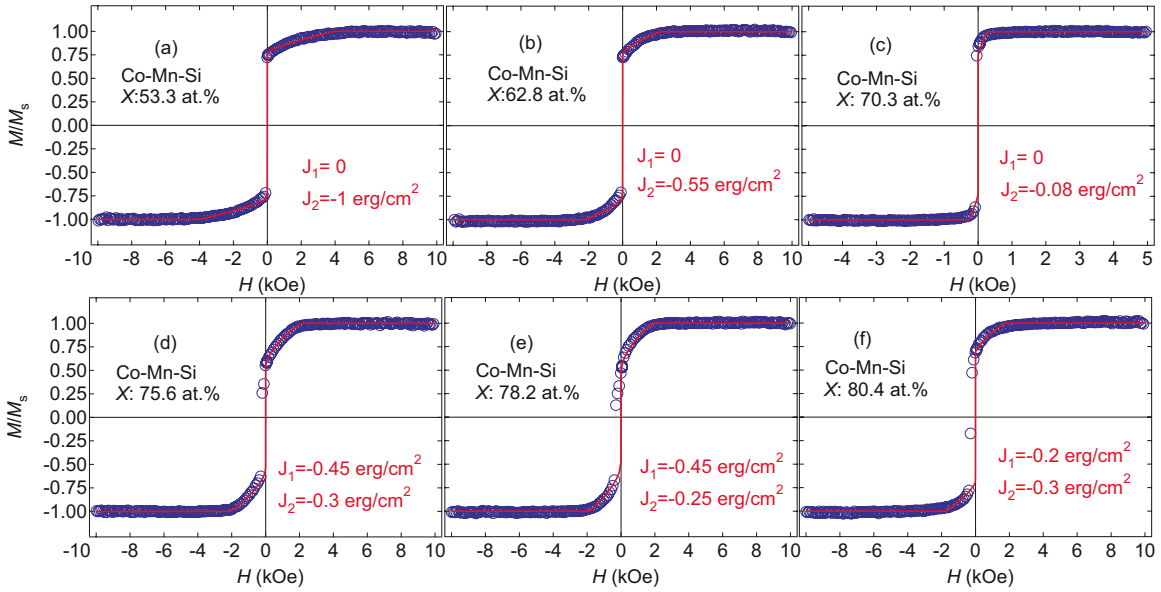

FIG. 9. (Color online) M-H loops of Co-Mn-Si(20 nm)/Cr(1.2 nm)/Co-Mn-Si(7 nm) trilayers for top and bottom Co-Mn-Si, X: (a) 53.3 at. %, (b) 62.8 at. %, (c) 70.3 at. %, (d) 75.6 at. %, (e) 78.2 at %, and (f) 80.4 at. %. The open circles and lines represent the experimental and numerical simulation results, respectively.

V. DISCUSSION

In the study of T_{ann} dependence, the crystal structure of CMS changes from a $B2$ ordered structure for as-deposited sample to a partially $L2_1$ ordered structure for samples post-annealed from 200 to 400 °C. However, there is no significant change in the magnetic properties; only 90° coupling dominates in all cases with almost the same strength. On the other hand, in the study of Co concentration dependence, the gradual increase in chemical disordering from $B2$ to $A2$ structure of Co-Mn-Si considerably affect the IEC behavior. The presence of 180° coupling has been observed only for highly Co antisite defective disordered ($A2$) structure, i.e., when more than 73% atoms are occupied by Co in Co-Mn-Si.

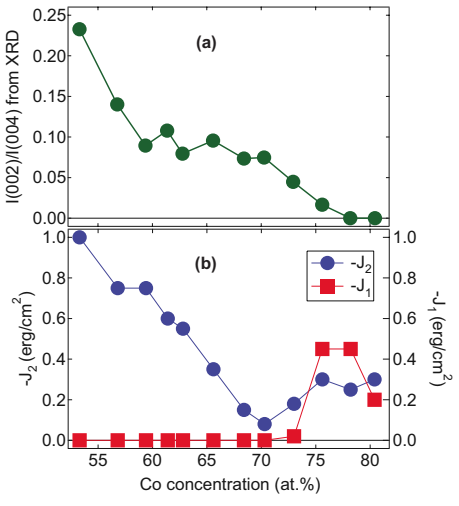

FIG. 10. (Color online) (a) Ratio of $B2$ superlattice peak to $A2$ fundamental peak intensities $I(002)/I(004)$ measured from XRD and (b) the values of J_1 and J_2 evaluated from numerical simulations as a function of Co concentration are plotted for a series of samples with different Co concentrations in Co-Mn-Si/Cr/Co-MnSi trilayers.

We will discuss our results of IEC in the view of existing models of 90° coupling. Concerning the so-called intrinsic theories,[14,33,34] which consider an ideal layered system without any interface roughness and chemical intermixing, calculations found that $|J_2|$ was much smaller than $|J_1|$ and it was significantly smaller than the values observed experimentally. The theories also predict that 90° alignments at zero magnetic field can be observed only for those spacer thicknesses at which the oscillating parameter J_1 has nodes. Therefore, we can easily exclude those models, as they have already failed to explain most of the experimental investigations of 90° coupling in different systems. Now we will focus on some familiar extrinsic models of 90° coupling such as magnetic-dipole mechanism,[35] Slonczewski's[36–38] predictions of fluctuation mechanism, loose spin mechanism and proximity magnetism of spacer material. According to magnetic-dipole mechanism, 90° coupling is completely related to the interface roughness and the strength of coupling is much small (0.01 erg/cm^2) even for very large roughnesses (period L=20–50 nm and height δ=0.5 nm of the interface roughness) and it is independent of spacer material. So we can also exclude this model as the strength of the 90° coupling is very large in comparison to the surface roughness in our samples. In another point of view, 90° coupling according to the fluctuation mechanism is associated with spatial fluctuations of bilinear coupling due to terraced variations in spacer thickness. However, the limitation of this model is that it cannot explain the 90° coupling itself only with no bilinear coupling, since the strength of the biquadratic coupling J_2 is directly related to the change in that of the bilinear coupling. Therefore it might be possible to make a simple explanation of our results for cases where both the 90° and bilinear couplings are existing. Furthermore, still

there are some misgivings of the strength of 90° coupling in such cases, since J_2 can only contribute in a minor way to the coupling. Another familiar model (of consideration) for 90° coupling is the loose spin model, based on magnetic impurity in spacer material and interfacial loose spins from ferromagnetic layers. However, it is also much too weak to account for the measured coupling strengths and oscillation of J_2 in CMS/Cr/CMS trilayers.[26] Finally, according to Slonczewski's another prediction in proximity magnetism of spacer, the existence of helicoidally twisted quasiantiferromagnetic proximity states in the Cr (Mn) lead to coupling energy completely different from the conventional coupling behavior as reported by Schreyer *et al.*[39] According to this model[38] the direct exchange between the antiferromagnetic spacer and the ferromagnetic layers at the ideally flat interfaces arises ferromagnetic and antiferromagnetic interlayer exchange coupling for odd and even number of monolayers of the spacer, respectively. However, in case of nonideal interfaces, i.e., due to the presence of one monolayer terraces at interfaces the magnetic frustration occurs. 90° coupling appears when both the ferromagnetic and antiferromagnetic exchange coupling parameters (C_+ and C_-) contribute equally, i.e., $C_+ = C_-$. The qualitative explanation of our observation might be possible using proximity magnetism model, but it cannot explain the origin of our present investigation which shows clear relation between the IEC and the degree of long-range $B2$ ordering with Co concentrations in Co-Mn-Si. A very recent theoretical investigation based on Slonczewski's proximity magnetism model by Kakeno *et al.*[40] predicted that the magnetic exchange interaction at the interface between the antiferromagnetic Cr spacer and ferromagnetic full-Heusler alloy shows completely different behavior from that between Cr and ferromagnetic transition-metal Fe. According to this calculation, the energetically stable condition for magnetic exchange interaction at the interface between Cr and CMS is not the same for Co- and Mn-Si-terminated interfaces. The Cr moments couple ferromagnetically with Co moments in Co-terminated interface, whereas, they (Cr moments) couples antiferromagnetically with Mn moments in Mn-Si-terminated interface. In our samples, CMS and Cr are grown epitaxially in (001) direction where Co and Mn-Si layers in CMS appear periodically. Therefore, in case of the presence of one monolayer terraces of $B2$ ordered CMS or antiphase boundaries at the interface both of the magnetic elements (Co and Mn) are available, giving rise to different type of magnetic frustration than that in Fe/Cr interface. Thus due to the opposite magnetic exchange interactions of Cr with two different magnetic elements (Co and Mn) and in turn the originating special magnetic frustration at the interface may cause the dominating 90° coupling in ordered full-Heusler alloy-based structures. This speculation is consistent with our observation where the degree of $L2_1$ ordering does not affect the strength of 90° coupling, where as, the enhancement of $A2$ disordering with Co concentrations in Co-Mn-Si reduce the strength (of 90° coupling). Moreover, it is to be noted here that, in our recent investigation of IEC in Co-Fe/Cr/Co-Fe trilayer structures [41]considerable the enhancement of 90° coupling strength has also been observed for the sample as deposited (at RT) to bottom Co-Fe $T_{ann} = 400$ °C, despite considerably small surface roughness. This seems to be due to the enhancement of $B2$ ordering of Co-Fe after annealing, where the different magnetic interaction of Co and Fe with Cr originates the same type of magnetic frustration at the interface as in Co-Mn-Si. However, the absence of 180° coupling and the long-period oscillation of only 90° coupling in ordered full-Heusler alloy-based structures are still mysterious. Therefore, more theoretical and experimental works are required to clarify the understanding of the effect of $B2$ ordering on IEC in full-Heusler alloy-based systems.

VI. SUMMARY

In conclusion, we have investigated structural and magnetic properties in Co_2MnSi-based fully epitaxial trilayers by changing the T_{ann} of bottom CMS and by preparing Co antisite defective Co-Mn-Si, systematically. The magnetization behavior has been simulated by using a numerical-simulation model, which shows a clear chemical-ordering dependence of IEC. The T_{ann} up to 400 °C, accordingly the chemical ordering of bottom CMS in CMS/Cr/CMS trilayers form completely $B2$ structure in as deposited (at RT) to partially $L2_1$ structure at $T_{ann} > 200$ °C does not affect the IEC, only 90° coupling appears in all cases. X-ray diffraction, AFM results, and composition analyses by ICP and EPMA in the Co concentration dependence study confirm the gradual change in Co concentration, accordingly the growth of chemically disordered Co-Mn-Si from $B2$ to $A2$ structure with increasing Co concentration in Co-Mn-Si/Cr/Co-Mn-Si trilayers keeping epitaxial growth and small surface roughnesses. The strength of 90° coupling is found to decrease monotonically with the Co concentration in turn decreasing the long-range $B2$ ordering and a strong contribution of 180° coupling appears for highly Co-antisite defective (disordered in $A2$ structure) Co-Mn-Si structures only. The interface exchange interaction between ordered full-Heusler structure and Cr spacer might play an important role in dominating 90° coupling in such structures. Finally, it would be interesting to see if any future theoretical coupling models can reproduce our observation.

ACKNOWLEDGMENTS

This work was performed under the cooperative research program of the Advanced Research Center of Metallic Glasses, Institute for Materials Research, Tohoku University. We gratefully acknowledge financial supports of this work from Grant-in-Aid for scientific Research in Priority Area "Creation and control of spin current" (Grant No. 19048004) and Young Scientists (B) (Grant No. 20760005) by MEXT, Japan. This work was supported in part by Global COE Program "Materials Integration (International Center of Education and Research), Tohoku University, MEXT, Japan. We would like to give thanks to J. Inoue, Nagoya University, for his interest in our work and support regarding theoretical analysis and M. Takeda of JAEA for PNR analysis.

[1] P. Grünberg, R. Schreiber, Y. Pang, M. B. Brodsky, and H. Sowers, Phys. Rev. Lett. **57**, 2442 (1986).
[2] M. N. Baibich, J. M. Broto, A. Fert, F. Nguyen Van Dau, F. Petroff, P. Eitenne, G. Creuzet, A. Friederich, and J. Chazelas, Phys. Rev. Lett. **61**, 2472 (1988).
[3] S. S. P. Parkin, N. More, and K. P. Roche, Phys. Rev. Lett. **64**, 2304 (1990).
[4] M. Rührig, R. Schäfer, A. Hubert, R. Mosler, J. A. Wolf, S. Demokritov, and P. Grünberg, Phys. Status Solidi A **125**, 635 (1991).
[5] S. S. P. Parkin, Phys. Rev. Lett. **67**, 3598 (1991).
[6] Q. Leng, V. Cros, R. Schafer, A. Fuss, P. Grünberg, and W. Zinn, J. Magn. Magn. Mater. **126**, 367 (1993).
[7] A. A. Rzhevsky, B. B. Krichevtsov, D. E. Burgler, and C. M. Schneider, Phys. Rev. B **75**, 144416 (2007).
[8] C. M. Schmidt, D. E. Bürgler, D. M. Schaller, F. Meisinger, and H. J. Güntherodt, Phys. Rev. B **60**, 4158 (1999).
[9] J. Unguris, R. J. Celotta, D. A. Tulchinsky, and D. T. Pierce, J. Magn. Magn. Mater. **198-199**, 396 (1993).
[10] J. J. Krebs, G. A. Prinz, M. E. Filipkowski, and C. J. Gutierrez, J. Appl. Phys. **79**, 4525 (1996).
[11] M. E. Filipkowski, J. J. Krebs, G. A. Prinz, and C. J. Gutierrez, Phys. Rev. Lett. **75**, 1847 (1995).
[12] P. Bruno and C. Chappert, Phys. Rev. B **46**, 261 (1992).
[13] P. Bruno, J. Phys.: Condens. Matter **11**, 9403 (1999).
[14] R. P. Erickson, B. Kristl Hathaway, and James R. Cullen, Phys. Rev. B **47**, 2626 (1993).
[15] S. O. Demokritov, J. Phys. D **31**, 925 (1998).
[16] Iosif Galanakis and Peter H. Dederichs, *Half-Metallic Alloys: Fundamentals and Applications*, Lecture Notes in Physics Vol. 676, edited by I. Galanakis and P. Dederichs (Springer, Berlin, 2005), pp. 1–39, and references therein.
[17] S. Fujii, S. Sugimura, S. Ishida, and S. Asano, J. Phys.: Condens. Matter **2**, 8583 (1990).
[18] S. Picozzi, A. Continenza, and A. J. Freeman, Phys. Rev. B **66**, 094421 (2002).
[19] Y. Sakuraba, M. Hattori, M. Oogane, Y. Ando, H. Kato, A. Sakuma, T. Miyazaki, and H. Kubota, Appl. Phys. Lett. **88**, 192508 (2006).
[20] Y. Sakuraba, J. Nakata, M. Oogane, H. Kubota, Y. Ando, A. Sakuma, and T. Miyazaki, Jpn. J. Appl. Phys., Part 2 **44**, L1100 (2005).
[21] K. Yakushiji, K. Saito, S. Mitani, K. Takanashi, Y. K. Takahashi, and K. Hono, Appl. Phys. Lett. **88**, 222504 (2006).
[22] Y. Sakuraba, T. Iwase, K. Saito, S. Mitani, and K. Takanashi, Appl. Phys. Lett. **94**, 012511 (2009).
[23] T. Iwase, Y. Sakuraba, S. Bosu, K. Saito, S. Mitani, and K. Takanashi, Appl. Phys. Express **2**, 063003 (2009).
[24] A. Bergmann, J. Grabis, B. P. Toperverg, V. Leiner, M. Wolf, H. Zabel, and K. Westerhalt, Phys. Rev. B **72**, 214403 (2005).
[25] T. Ambrose, J. J. Krebs, and G. A. Prinz, J. Appl. Phys. **89**, 7522 (2001).
[26] H. Wang, A. Sato, K. Saito, S. Mitani, K. Takanashi, and K. Yakushiji, Appl. Phys. Lett. **90**, 142510 (2007).
[27] H. Wang, S. Mitani, A Sato, K. Saito, K. Takanashi, and K. Yakushiji, J. Appl. Phys. **101**, 09J510 (2007).
[28] S. Bosu, Y. Sakuraba, K. Saito, H. Wang, S. Mitani, and K. Takanashi, J. Phys.: Conf. Ser. **83**, 012013 (2007).
[29] S. Bosu, Y. Sakuraba, K. Saito, H. Wang, S. Mitani, and K. Takanashi, IEEE Trans. Magn. **44**, 2620 (2008).
[30] S. Bosu, Y. Sakuraba, K. Saito, H. Wang, S. Mitani, and K. Takanashi, J. Appl. Phys. **105**, 07C710 (2009).
[31] S. Bosu, Y. Sakubara, M. Takeda, K. Saito, H. Wang, and K. Takanashi (unpublished).
[32] Y. Sakuraba, K. Takanashi, N. Hirose, M. Oogane, Y. Ando, and T. Nakamura, Appl. Phys. Lett. (to be published).
[33] J. Inoue, J. Magn. Magn. Mater. **136**, 233 (1994).
[34] D. M. Edwards, J. M. Ward, and J. Mathon, J. Magn. Magn. Mater. **126**, 380 (1993).
[35] S. Demokritov, E. Tsymbal, P. Grünberg, W. Zinn, and Ivan K. Schuller, Phys. Rev. B **49**, 720 (1994).
[36] J. C. Slonczewski, Phys. Rev. Lett. **67**, 3172 (1991).
[37] J. C. Slonczewski, J. Appl. Phys. **73**, 5957 (1993).
[38] J. C. Slonczewski, J. Magn. Magn. Mater. **150**, 13 (1995).
[39] A. Schreyer, J. F. Ankner, Th. Zeidler, H. Zabel, M. Schäfer, J. A. Wolf, P. Grünberg, and C. F. Majkrzak, Phys. Rev. B **52**, 16066 (1995).
[40] W. Kakeno, S. Honda, H. Itoh, and J. Inoue (unpublished).
[41] S. Bosu, Y. Sakuraba, K. Saito, H. Wang, and K. Takanashi (unpublished).